Crystallization behaviour of poly(ether-ether-ketone)

Peggy Cebe* and Su-Don Hong†
Applied Sciences and Microgravity Experiments Section, Jet Propulsion Laboratory, California Institute of Technology, Pasadena, CA 91109, USA
(Received 23 September 1985; revised 6 January 1986)

A study has been made of the crystallization behaviour of poly(ether-ether-ketone), PEEK, under isothermal and non-isothermal conditions. A differential scanning calorimeter was used to monitor the energetics of the crystallization process from the melt and from the rubbery amorphous state. During isothermal crystallization, relative crystallinity develops with a time dependence described by the Avrami equation, with exponent $n=3$. Greater absolute crystallinity develops during melt crystallization, nearly twice that which develops from the rubbery state, for comparable rates of crystallization. For non-isothermal studies, amorphous films were crystallized by heating or cooling at rates from 1°C/min to 50°C/min. A large fraction of crystallinity, from 0.45 to 0.70, develops by secondary processes. A kinetic treatment based on the Avrami equation is presented to describe the primary processes leading to non-isothermal crystallization. We have calculated activation energies of 68 kcal mol^{-1} for crystallization from the melt, and 52 kcal mol^{-1} for crystallization from the rubbery amorphous state. Results of isothermal and non-isothermal crystallization of PEEK are compared with those of poly(ethylene terephthalate).

(Keywords: poly(aryl-ether-ether-ketone); crystallization; differential scanning calorimetry)

INTRODUCTION

Poly(ether-ether-ketone), PEEK, is a crystallizable high performance thermoplastic having a high yield stress, Charpy impact strength of 54 kJ/mm[1], and a continuous service temperature of 200°C[2]. These properties make PEEK an attractive high performance polymer for potential structural adhesive and composite matrix applications. PEEK has excellent solvent resistance, being completely soluble at room temperature only in concentrated sulphuric acid[2,3]. While this is an attractive property when PEEK is used in hostile environments, it means that bulk processing must be done from the melt. To obtain melt pressed films, temperatures from 370°C to 400°C must be used, and commercially available PEEK material (from ICI, Americas Inc.) withstands these temperatures well.

PEEK can be obtained as amorphous or semicrystalline film, depending on the processing conditions from the molten state[4,5]. Amorphous material is obtained by rapidly quenching the melt. This material has a density of 1.264 g/cc as reported by Hay *et al.*[5], or 1.263 g/cc according to Blundell and Osborn[4]. The crystalline form can be obtained by slow cooling the melt, or by isothermal crystallization at a temperature between the crystal melting point and T_g. The amorphous film may also be crystallized from the rubbery state by heating above T_g[4,5]. The cold crystallization exotherm has been reported previously[4], occurring at 180°C when an amorphous film was heated at 20°C/min in a scanning calorimeter.

The crystal structure has been studied and reported in the literature[4-6]. Dawson and Blundell[6] reported the orthorhombic cell parameters to be $a=7.75$ Å, $b=5.86$ Å and $c=10.00$ Å, whereas Hay *et al.*[5], using a refined procedure to determine crystal structure, reported the cell parameters to be: $a=7.781$ Å, $b=5.922$ Å and $c=10.056$ Å. As a result of the differing cell parameters, there are two different values for the crystal density reported: 1.400 g/cc[4,6] and 1.378 g/cc[5]. The crystal melting point is reported to be 335°C, and T_g is 145°C[2,4].

Studies of crystallization of PEEK have been concerned with the rate of growth, surface free energies and morphology of PEEK crystallized isothermally at different temperatures[4,7]. The study of Blundell and Osborn[4] deals with formation and growth of spherulites in specially prepared PEEK material having a greatly reduced nucleation density. Details of this preparation were not reported, and this makes comparative studies difficult since commercially available PEEK crystallises in a fine grained mosaic structure with spherulites too small to be observed optically. *In situ* measurements of growth rate by optical microscopy could not be applied to this material.

In this study we have used differential scanning calorimetry, d.s.c., to measure the heat evolved during crystallization. The Avrami equation[8] was used to analyse the isothermal crystallization during the primary crystallization process. Several studies of rate dependent crystallization were undertaken to investigate the cold crystallization behaviour of samples subjected to successive heating cycles. A study of crystallization of PEEK under non-isothermal conditions is reported for heating and cooling rates from 1°C/min to 50°C/min.

EXPERIMENTAL

Samples used in this study were pressed from as-received pellets of PEEK (from ICI, Americas Inc.). Pellets had a relative viscosity of 2.4 when measured in 96% H_2SO_4, at

*NASA-NRC Resident Research Associate.
†Current address: 1625 Olympic Blvd., Suite 800, Los Angeles, CA, 90015, USA.

0032-3861/86/081183-10$03.00

25°C, 1 g/100 ml concentration. Pellets were dried under vacuum at 110°C before being pressed into films. A Pasadena Hydraulic Press was used to form films approximately 0.010 inches thick. Pressing was done at 370°C under 2.9 MPa pressure for two minutes. Films were quenched into a water bath to form amorphous PEEK, of density 1.265 g/cc. While this amorphous density is slightly higher than that reported previously, 1.264 g/cc[5], wide-angle X-ray scattering curves of these films appeared to be completely amorphous. Subsequent thermal treatments were used to impart crystallinity to the films.

The absolute degree of crystallinity was found from density measurements, assuming 1.378 g/cc as the density of the perfectly crystalline material[5], and 1.264 g/cc for the amorphous density. A Mettler FP80 hot stage was used to crystallize samples for the density measurements. The results obtained from density were in good agreement with those determined from the area under the d.s.c. endotherm. To calculate the degree of crystallinity from the endotherm, a value of 130 J/g was assumed for the heat of fusion of the perfect crystal[4].

A Dupont 1090 thermal analyser was used to monitor the heat flow from the sample during crystallization. Isothermal crystallization was carried out by cooling the melt or by heating the amorphous film above the glass transition temperature. The high temperature crystallization was carried out by first heating the sample to 400°C for several minutes to melt it, then cooling quickly to the crystallization temperature. For crystallization at low temperature, the sample was inserted into the calorimeter cell which was already heated to the crystallization temperature. Heat flow after sample insertion is shown in *Figure 1* for isothermal crystallization at 164°C. Crystallization begins at A, preceded by a short period in which the sample equilibrated at the crystallization temperature. Increasing heat flow from the sample is recorded until the maximum is reached at B. Crystallization slows down beyond B, and the measurement is terminated when no more heat flows from the sample. The relative degree of crystallinity as a function of time, $X_c(t)$, was found from:

$$X_c(t)/X_c(\infty) = \int_0^\infty \dot{Q}(t)\mathrm{d}t \qquad (1)$$

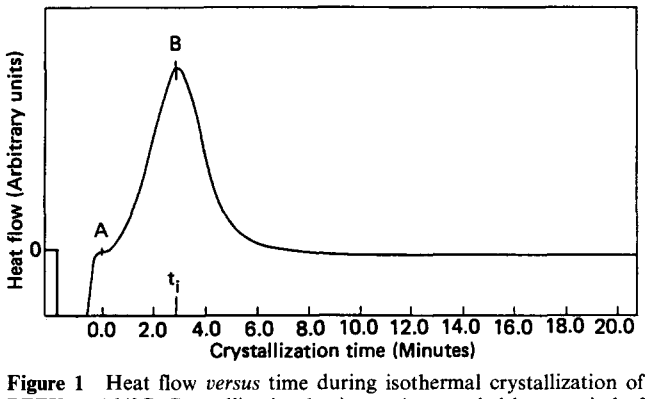

Figure 1 Heat flow *versus* time during isothermal crystallization of PEEK at 164°C. Crystallization begins at A, preceded by a period of equilibration at the crystallization temperature. Point B marks the change to a slower kinetic process and occurs at time t_i beyond the start of crystallization

Table 1 Relative and absolute crystallinity at t_i and t_c respectively

T (°C)	t_i[a] (min)	t_c[b] (min)	Crystallinity at t_c $X_c(\infty)$ (%)	Rel. crystallinity at t_i $X_c(t_i)/X_c(\infty)$
315	16.0	60	35	0.49
312	7.4	40	34	0.48
308	3.8	20	34	0.50
164	2.7	20	18	0.44
160	11.6	32	16	0.47

[a] t_i and $X_c(t_i)$ are the time and degree of crystallinity at $\mathrm{d}\dot{Q}/\mathrm{d}t = 0$
[b] t_c is the crystallization time

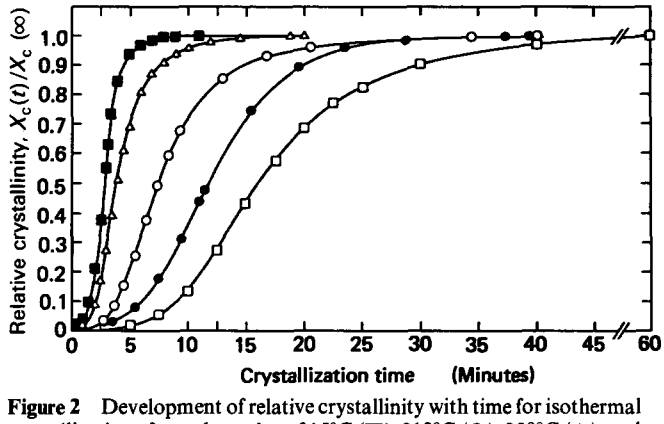

Figure 2 Development of relative crystallinity with time for isothermal crystallizations from the melt at 315°C (□), 312°C (○), 308°C (△), and from the rubbery amorphous state at 164°C (■) and 160°C (●)

where $X_c(\infty)$ is the ultimate crystallinity at very long times, and $\dot{Q}(t)$ is the heat flow rate. $X_c(\infty)$ was found from the density of the isothermally crystallized samples.

In the case of non-isothermal crystallizations, the d.s.c. was used to provide a constant rate of change of temperature and to monitor the heat flow as a function of temperature. Rates of heating and cooling ranged from 1°C/min to 50°C/min.

RESULTS

Isothermal crystallization kinetics of PEEK

Table 1 presents a summary of crystallinity and time data for isothermal crystallizations from the melt and from the rubbery amorphous state. The time t_i represents the time to reach the maximum rate of heat flow, and corresponds to the change-over to a slower kinetic process, due to impingement of adjacent spherulites[4]. Crystallization continues until the time t_c after which no futher heat flow is observed. The fraction of crystallinity that develops by the time t_i is shown in the last column of *Table 1*. The relative amount of crystallinity that developed at time t_i is slightly larger for the high temperature crystallizations than for crystallization from the rubbery amorphous state. The relative amount of crystallinity has been plotted in *Figure 2* for the five crystallization temperatures. Development of the relative crystallinity can be analysed using the Avrami equation[8]:

$$X_c(t)/X_c(\infty) = 1 - \exp(-kt^n) \qquad (2a)$$

$$\ln(1 - X_c(t)/X_c(\infty)) = -kt^n \qquad (2b)$$

where n is a constant whose value depends on the mechanism of nucleation and on the form of crystal

growth, and k is a constant containing the nucleation and growth parameters. Plots of $\log(-\ln[1-X_c(t)/X_c(\infty)])$ vs. $\log t$ are shown in *Figure 3*. Each curve has a linear portion followed by a gentle roll-off at longer times. Four of the curves depart from linearity in the short-time region where the logarithmic plotting tends to exaggerate small errors in the assignment of the start of crystallization. The roll-off at longer time begins at a lower degree of conversion for the melt crystallization compared with cold crystallization. For the three high temperature crystallizations, a linear trend is observed at long times but with reduced slope compared to that of the primary crystallization process, a point we will return to later. At high temperatures, the change to a secondary kinetic process is more abrupt than for the low temperature crystallization.

Fitting the initial linear portion of $\log(-\ln[1-X_c(t)/X_c(\infty)])$ vs. $\log t$ for times before the roll-off allows us to determine n and k from equation (2). The values are listed in *Table 2*. Since t_i is the solution of $d^2X/dt^2 = 0$, we can use equation (2) to write t_i in terms of n and k, obtaining:

$$t_i = ((n-1)/nk)^{1/n} \quad (3)$$

The calculated values of t_i listed in *Table 2* can be compared with the t_i obtained directly from the plots of $\dot{Q}$ vs. t, as listed in *Table 1*. The agreement in t_i values suggests that the Avrami analysis works well in describing the initial development of crystallinity, whether from the melt or from the rubbery amorphous state. The exponent n, obtained from the Avrami analysis, has a value of about 3.0. The narrow spread in n values centred around 3.0 in such a wide crystallization temperature range indicates

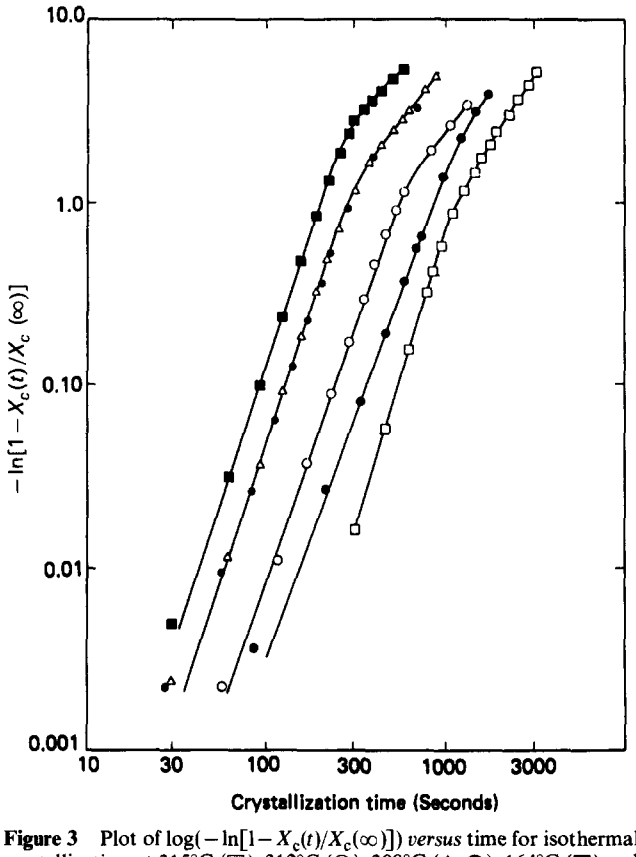

Figure 3 Plot of $\log(-\ln[1-X_c(t)/X_c(\infty)])$ *versus* time for isothermal crystallization at 315°C (□), 312°C (○), 308°C (△,●), 164°C (■) and 160°C (●)

Table 2 Parameters n and k from the Avrami analysis of isothermal crystallization

T (°C)	n	k	t_i[a] (minutes)
315	3.3	8.0×10^{-5}	15.9
312	3.0	1.7×10^{-3}	7.3
308	3.05	1.0×10^{-2}	3.9
164	3.0	3.1×10^{-2}	2.8
160	2.8	6.7×10^{-4}	11.4

[a] Calculated from equation (3)

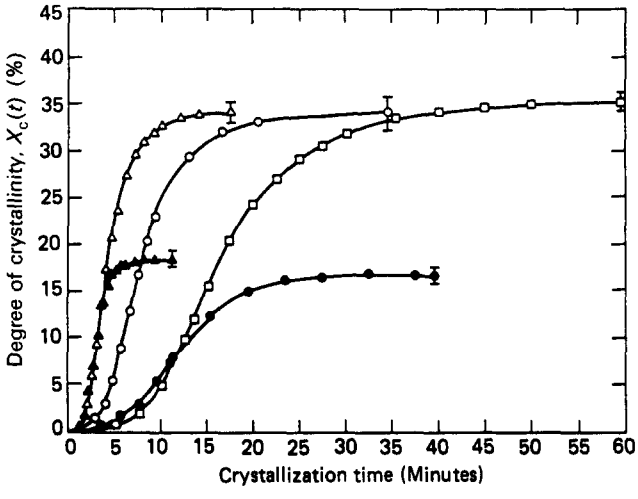

Figure 4 Development of absolute crystallinity with time for isothermal crystallization at 315°C (□), 312°C (○), 308°C (△), 164°C (▲) and 160°C (●)

that the nucleation process is simultaneous, and the growth of crystals in PEEK is probably spherulitic[9]. Using polarizing optical microscopy, we were unable to see spherulites in ICI PEEK, even at 800× magnification. However, poly(ether-ether-ketone) synthesized in our laboratory according to the method of Attwood[2] could be crystallized readily in the form of large spherulites 5–250 μm in diameter[10]. When synthesized PEEK was cooled from 350°C, only a fine grained mosaic structure could be observed similar to that seen in commercial ICI PEEK. Melting at 370°C resulted in the large spherulite structures, and is an indication that the nucleation density has been reduced at a melt temperature of 370°C. Absence of spherulites large enough to be detected by optical microscopy leads us to believe that the ICI PEEK is crystallizing heterogeneously by simultaneous formation of many nuclei. ICI PEEK had a distinct dark grey colour and this may indicate the presence of a nucleating agent.

The Avrami analysis describes the development of the relative crystallinity, $X_c(t)/X_c(\infty)$. While this is satisfactory for determining the primary crystallization kinetics, it ignores the very large differences in $X_c(\infty)$ that occur in the high and low temperature crystallization. In *Figure 4* we have plotted the absolute crystallinity $X_c(t)$ by scaling the curves of *Figure 2* with $X_c(\infty)$. High and low temperature isothermal crystallizations are not equivalent even when the rates of completion of crystallization are comparable. For instance, the data for 160°C crystallization shown in *Figure 3* are bracketed by the 312°C and 315°C data indicating that the rate of completion for 160°C is intermediate between the rates for

312°C and 315°C. But from *Figure 4* it is apparent that about half as much material crystallizes at the low temperatures.

Effect of thermal history on PEEK crystallization and melting

Widely varying thermal treatments were used to study the effect of heating and cooling rate on subsequent endothermic response. D.s.c. scans at 20°C/min heating rate are shown in *Figure 5* for three sample treatments: fast quenching from the melt, isothermal crystallization at high temperature and slow cooling from the melt. Curve A represents the response of melt quenched amorphous PEEK when heated from 70°C to 400°C. The glass transition at 145°C is followed by a sharp exotherm at 180°C, as previously reported[4,6]. Crystallization continues up to about 270°C but with diminished heat flow. A broad endotherm with peak at 335°C indicates that a broad distribution of crystal sizes is present in the material after crystallization. The area under the exotherm can be compared with that under the endotherm, to estimate the fraction of crystals in the sample at room temperature. Using 130 J/g as the heat of fusion of perfectly crystalline PEEK[4], and making the assumption that the heat of fusion is the same as the heat of crystallization, we find that the degree of crystallinity that develops by crystallization during the scan is 20.6%, compared with 22.0% calculated from the melting endotherm. The difference of 1.4% may be viewed as the amount of crystallinity that existed in the sample at room temperature.

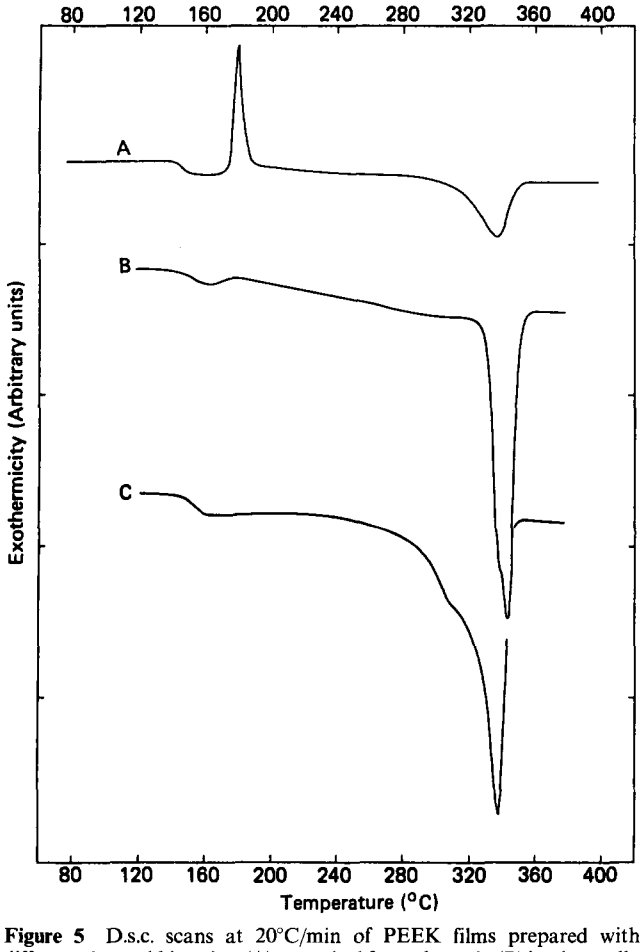

Figure 5 D.s.c. scans at 20°C/min of PEEK films prepared with different thermal histories: (A) quenched from the melt, (B) isothermally crystallized from the melt at 314°C for 17 h and (C) cooled very slowly from the melt

Within the limits of error in determining the areas, we can say that the melt quenched sample was nearly amorphous at room temperature, and all crystallinity developed during the d.s.c. scan. Thus, even though the main exotherm is appearing just above the glass transition, the crystals formed at this low temperature thicken during the scan and melting at 335°C. The scanning rate of 20°C/min is not fast enough to prevent reorganization into more perfect crystals during the scan. However, even at a reduced scanning rate of 5°C/min, the thermal response had the same appearance as that shown in curve A. The crystals formed near 180°C during the scan do not melt at significantly lower temperature compared with crystals formed by other treatments to be described below.

Curve B in *Figure 5* is a d.s.c. scan of PEEK crystallized isothermally at 314°C for 17 h. The sample was removed from the press while hot and cooled in a few minutes to room temperature. T_g is shifted slightly towards higher temperature and is followed once again by an exotherm at 180°C, but this time the exotherm is diminished in size. It is remarkable that the sample shows any tendency to crystallize at low temperature given its long isothermal treatment at high temperature which allows the development of a large degree of crystallinity (31%). The endotherm has been shifted to a higher temperature, 342°C, and in its main body appears to be much narrower than the endotherm of the quenched amorphous sample. However, note that the peak has a low temperature shoulder about 335°C, and another smaller, but very broad, component located at 270°C–320°C. We assign the broad component endotherm to those crystals formed during cooling after the completion of the isothermal crystallization. The sharpness of the main endotherm would then be attributed to the melting of those crystals formed during the isothermal crystallization at high temperature.

A film slowly cooled from 370°C to room temperature over a period of 17 h produced the scan shown in curve C of *Figure 5*. After this treatment, no further crystallization occurs at 180°C. During the slow cooling, the film samples the entire range of temperature from 370°C to 25°C very slowly. All crystals that could form at 180°C did so during cooling, and subsequent heating did not induce any further low temperature crystallization. The endotherm in this case is extremely broad, with a distinct shoulder at about 310°C, and a sharp melting peak at 338°C. We found that all slow cooling treatments of the melt resulted in a low temperature shoulder on the melting endotherm. However, the exact location of the shoulder was sensitive to the cooling rate. Another sample (not shown in *Figure 5*) was cooled from the melt at a faster rate by removing the hot platens from the press. This sample cooled in about 3 h from 370°C to room temperature. Like the slowly cooled sample (curve C of *Figure 5*), this film had no low temperature exotherm at 180°C. Melting occurred over a broad temperature range, and the main endotherm was preceded by a broad secondary peak at 270°C.

Low temperature crystallization was investigated further by a series of crystallization treatments, and results are shown in *Figure 6*. An originally amorphous sample was heated to 210°C, then cooled and its exotherm recorded at 20°C/min scanning rate as shown in *Figure 6a*. The exothermic peak seen in *Figure 5*, curve A at

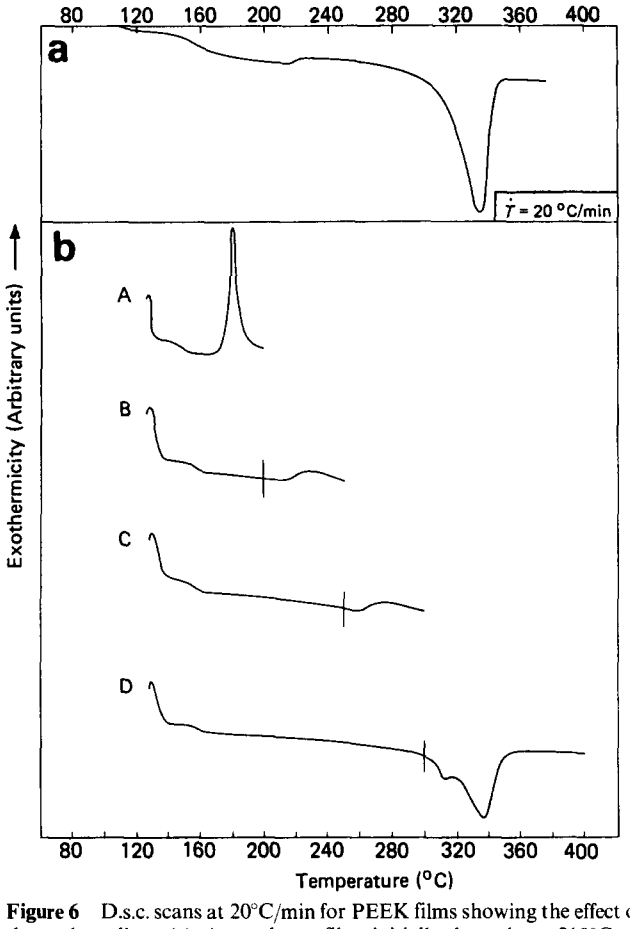

Figure 6 D.s.c. scans at 20°C/min for PEEK films showing the effect of thermal cycling. (a) Amorphous film initially heated to 210°C at 20°C/min, then cooled to room temperature and scanned; (b) amorphous film, scanned while heating to 200°C (curve A), cooled and reheated to 250°C (curve B), cooled and reheated to 300°C (curve C), cooled and reheated to 400°C (curve D)

180°C is now shifted to about 220°C, just above the heat treatment temperature. No secondary peaks occur on the endotherm as a result of this treatment at 210°C. To look for effects of thermal cycling, a similar series of heat treatments was conducted, and results are shown in *Figure 6b*. Curve A shows the initial scan of the amorphous sample up to the treatment temperature of 200°C. This curve is identical to *Figure 5* curve A up to 200°C. The sample was then cooled and reheated to 250°C, as shown in *Figure 6b*, curve B. A purely exothermic peak appears which is much smaller than the first exotherm at 180°C indicating a reduction in the amount of further crystallization upon heating to elevated temperatures. The exotherm has been shifted to 225°C, just above the heat treatment temperature of 200°C (indicated by the vertical marker). On the next reheating, the exotherm is pushed to a still higher temperature of about 270°C. Now, however, a very slight endothermic character is observed at about 255°C, followed immediately by a crystallization exotherm. The endotherm is the result of the melting of imperfect crystals formed near 250°C. These crystals melt just above their formation temperature, and reorganize into more perfect crystals during the scan. One final heating is shown in curve D, where the sample is now heated to 400°C. No exotherm is seen at any temperature, and only melting behaviour is observed. The melting endotherm is complicated by a secondary peak at 310°C which is just above the highest previous treatment temperature. Compare this behaviour with the melting endotherm in *Figure 6a* which has no secondary peaks. The heat treatment shown in curve C results in the development of a crystal population that melts below the temperature of the main endotherm. We have already seen that low temperature crystallization does not result in such a secondary peak, and conclude that the heat treatment from 250°C to 300°C has an annealing effect. Crystals which formerly melted on the low temperature side of the main endotherm are perfected by the successive heat treatments at higher temperature, and now melt at 310°C.

Rate-dependent crystallization

Crystallization of PEEK was studied under non-isothermal conditions of heating and cooling. Amorphous samples were crystallized by heating from 80°C to 280°C at rates ranging from 1°C/min to 50°C/min. At the lowest rates, the crystallization scan was terminated at temperatures lower than 280°C when no further exothermic departure from the baseline could be detected. Samples were then melted at 400°C for two minutes to ensure complete melting. The necessity of using a high temperature melting step is shown in *Figure 7*. The first scan is that of a sample heated to 400°C and held at 20 min, before cooling at 10°C/min to 250°C. The sample was immediately reheated at 10°C/min to 350°C and held isothermally for 2 min. The second cooling scan illustrates the effect of incomplete melting on the crystallization exotherm. Existence of crystal seeds in the melt results in initiation of crystallization at higher temperature. All subsequent results on melt crystallization were obtained on samples that experienced a melt of 400°C.

The results of the heating and cooling crystallization are shown in *Figures 8a,b* for several of the applied rates. The exothermic peak on heating, shown in *Figure 8a*, shifts to higher temperature as the heating rate increases, and becomes more broad. At 1°C/min, the peak temperature is about 164.4°C, increasing to 188.8°C at the highest heating rate of 50°C/min. On cooling, maximum rate of heat flow occurs at a temperature of 308°C for −1°C/min, and at 286°C for −20°C/min. This result differs from that of Blundell and Osborn who report an

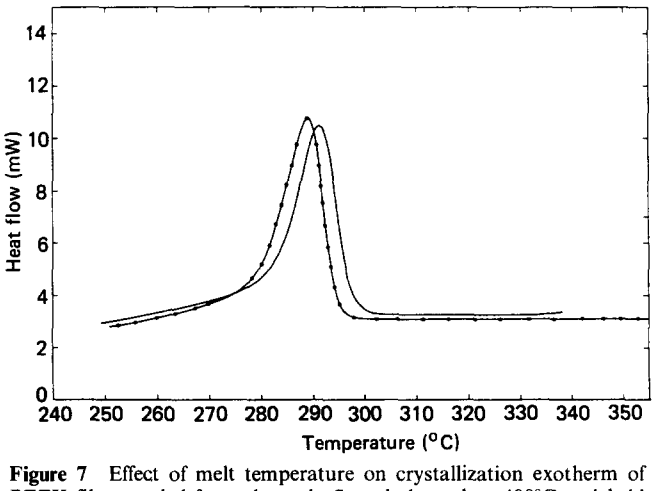

Figure 7 Effect of melt temperature on crystallization exotherm of PEEK films cooled from the melt. Sample heated to 400°C and held 20 min, then cooled at 10°C/min to 250°C (-●-). Sample reheated to 350°C, held 2 min, then cooled at 10°C/min to 250°C (———)

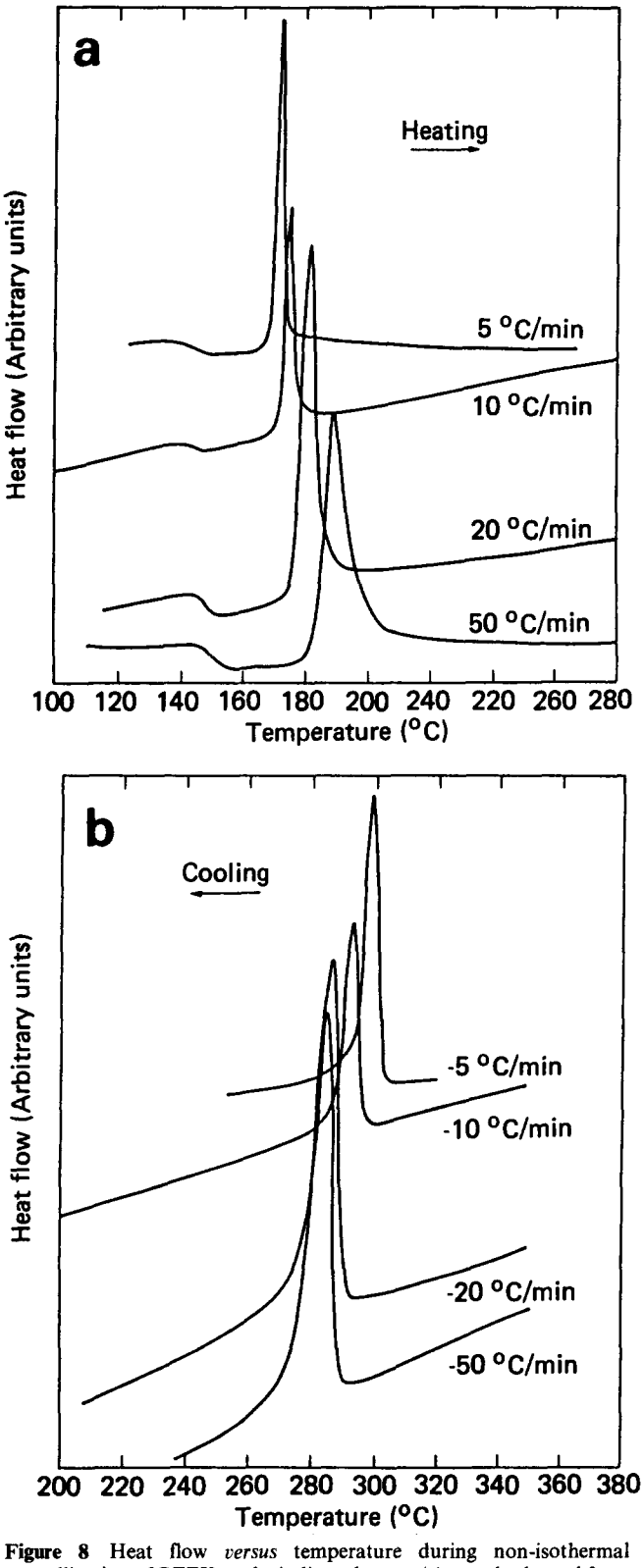

Figure 8 Heat flow *versus* temperature during non-isothermal crystallization of PEEK at the indicated rates: (a) samples heated from the rubbery amorphous state; (b) samples cooled from the melt

exothermic peak at 255°C when the melt is cooled at 20°C/min[4]. This difference may be due to the reduced nucleation density in the PEEK used by Blundell and Osborn. Values of temperature, time and relative crystallinity that develop at the maximum in the heat flow curve are listed in *Table 3*. It was not possible to control the sample temperature precisely when cooling at −50°C/min, hence the data at −50°C/min were not used in the kinetic analysis.

Integration of the exothermic peaks during the non-isothermal scan gives the relative degree of crystallinity as a function of temperature. These results are shown in *Figures 9a,b* for the heating and cooling programmes. Note that the abscissa for curves in *Figure 9* is temperature, whereas in the isothermal crystallization (*Figure 2*) it was time. The curves are horizontally shifted in temperature as a result of a rate-dependent induction time preceding the initiation of crystallization.

The inflection point t_i, in each curve represents the temperature corresponding to the maximum rate of heat flow (the peak temperatures in *Figure 8*). The inflection point occurs at decreasing degree of conversion as the heating/cooling rate increases. At +1°C/min, relative crystallinity is 0.48 at t_i, whereas it is only 0.24 at t_i when

Table 3 Temperature, time and relative crystallinity at maximum rate of heat flow during non-isothermal crystallization

Rate, ϕ (°C/min)	Temperature[a] T (°C)	Time[a] t_i (minutes)	$X_c(t_i)/X_c(\infty)$
−50	282.7	0.15	–
−20	284.0	0.50	0.33
−10	291.9	0.89	0.37
−5	297.0	1.63	0.43
−2	302.7	3.08	0.44
−1	308.0	3.24	0.42
+50	188.8	0.28	0.24
+20	182.3	0.62	0.35
+10	175.2	0.67	0.41
+5	171.3	2.26	0.41
+2	167.1	4.05	0.49
+1	164.4	6.90	0.48

[a] T and t_i are the temperature and time at $d\dot{Q}/dt = 0$, respectively

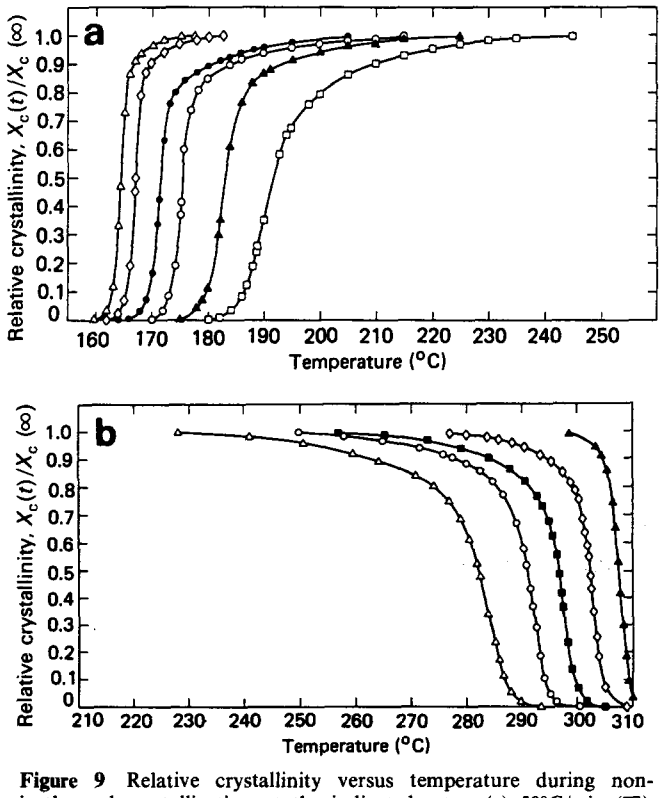

Figure 9 Relative crystallinity versus temperature during non-isothermal crystallization at the indicated rates: (a) 50°C/min (□), 20°C/min (▲), 10°C/min (○), 5°C/min (●), 2°C/min (◇), 1°C/min (△); (b) −20°C/min (△), −10°C/min (○), −5°C/min (■), −2°C/min (◇), −1°C/min (▲)

the rate was increased to +50°C/min. For the cooling curves, the relative crystallinity that develops at t_i is 0.42 at −1°C/min, decreasing to 0.33 at −20°C/min. As the rate of change of temperature increases, a larger relative amount of crystallization occurs after the inflection point.

DISCUSSION

Isothermal crystallization

We can use the rate constant, k, determined from the Avrami analysis to gain further insight into PEEK crystallization in the high temperature regime from 308°C to 315°C. We assume that the crystallization at high temperature follows the Hoffman–Lauritzen equation for secondary growth and heterogeneous nucleation[12]. Following previous treatments[4,13,14] we write the growth equation:

$$G = G_0 \exp[-U/R(T-T_\infty)]\exp[-KT_m/T\Delta T] \quad (4)$$

where

$$K = 4b\sigma\sigma_e/\Delta hk$$

In equation (4), U is the transport activation energy, T_m is the infinite crystal melting point, ΔT is the degree of undercooling, and T_∞ is chosen as $T_\infty = (T_g - 51.6)$[4]. The kinetic parameter K contains the surface free energy product, $\sigma\sigma_e$, and Δh, the heat of fusion of a perfect crystal, and is derived from plots of $\log G + U/R(T-T_\infty)$ vs. $T_m^2/T\Delta T$.

The linear growth rate G is related to the Avrami parameter k by $G \sim k^{1/n}$ where n is the Avrami exponent. Choosing $U = 2$ kcal mol^{-1} and $T_m = 668$ K, our data gave a slope of $K = -660$ K. This result is in very good agreement with that of Blundell and Osborn[4] ($K = -590$ K, from Figure 7, ref. 4) using growth rate data derived from measurement of the average spherulite diameter that had developed by the time t_i. The special PEEK used by Blundell and Osborn[4] had a very low nucleation density, and was treated assuming homogeneous nucleation. In spite of this, growth rates determined by two different methods led to similar values of K.

The initial development of crystallinity in PEEK follows the Avrami equation in its time dependence, and this is shown to hold over the region from the beginning of crystallization until the roll-off to a secondary process. The Avrami exponent n was about 3 for both high and low temperature isothermal crystallization. The result agrees with the cold crystallization data presented by Kemmish and Hay[11]. It is useful to compare the isothermal crystallization behaviour of PEEK with that of its chemical relative PET, poly(ethylene terephthalate)[15–17]. High temperature isothermal crystallizations of PET were carried out by Vilanova *et al.*[15]. Vilanova finds an Avrami exponent of $n = 2$–3 for melt crystallization of low molecular weight fractions of PET, and $n \sim 3$ for the unfractionated polymer. PEEK and PET behave similarly when crystallized from the melt in terms of their Avrami exponents. However, the low temperature 'cold' crystallization behaviours are quite different. From the experiments of Miller[16] and Mayhan *et al.*[17], it has been determined that PET follows a first order rate equation for the primary 'cold' crystallization process. The rate law used to describe PET crystallization from the rubbery amorphous state was of the form:

$$da/dt = K(T)[1-a]^p \quad (5)$$

where $a = X_c(t)/X_c(\infty)$, $K(T)$ is a reaction rate, and $p = 1$ for the first order reaction. By integration, equation (5) can be cast in the form: $\ln(1-a) = K(T)t$. Comparing this with equation (2b), we see that in the case of $p = 1$, the time development of crystallinity is identical to a process described by the Avrami equation with an Avrami exponent of $n = 1$. This means that for PET crystallized isothermally at low temperature, the crystallinity develops with a slower time response ($\sim t$) when compared with the time response of PEEK ($\sim t^3$).

Effects of thermal history

Results of the effect of thermal history on the crystallization of PEEK were shown in *Figures 5–7*. These results can be summarized as follows. Samples quenched from high temperature will crystallize just above T_g when the sample is subsequently scanned in the d.s.c. (*Figure 5*, curve A). A scanning rate of 20°C/min was chosen to minimize the reorganization of these crystals during the scan. The crystals formed at 180°C during the scan melt over a broad range of temperatures, with a peak at about 335°C. Samples partially crystallized at high temperature 314°C for long times may undergo further crystallization at 180°C when they are scanned if the cooling rate was fast enough to prevent complete crystallization (*Figure 5*, curve B). Crystallization at high temperature does not preclude further crystallization at much lower temperatures. However, the shape and position of the endotherm are very different from that of the originally amorphous material. High temperature crystallization results in more perfect crystals that melt over a narrow range of temperatures, with a higher endothermic peak at 342°C. The crystals formed at low temperature during the scan melt in the range from 270°C to 310°C giving a broad flat component to the endotherm.

Any treatment which involves slow cooling from the melt, as opposed to quenching, will allow more complete crystallization during cooling. No low temperature exotherm will be seen when these samples are subsequently heated (*Figure 5*, curve C). The crystals formed at a high degree of undercooling in a partially crystallized sample are very small and imperfect, and occur between existing lamellae. They contribute a broad component in the d.s.c. scan at low temperatures, beginning at 250°C with a peak at 310°C. The position of the main endotherm is 335°C, the same as for the originally amorphous material which crystallized during the scan.

Effects of thermal cycling were shown in *Figure 6*. Heating to 210°C, followed by scanning to 380°C, showed that further crystallization occurs above the treatment temperature, but the main endotherm consists of a single peak (*Figure 6a*). Repetitive treatment at successively higher temperatures show crystallization occurring at 260°C–280°C (*Figure 6b*). Whereas most of the crystals formed at 180°C melt at 335°C (*Figure 5*, curve A), the successive heat treatments at high temperature result in a secondary endotherm at 310°C (*Figure 6b*, curve D). Increases in crystallinity result when the treatment temperature increases, as shown in *Figure 3* for different rates.

The results shown in *Figure 6* can be compared with the behaviour reported by Blundell and Osborn[4] for isothermal crystallization in the temperature range from 230°C to 270°C. In that study, samples of melt quenched amorphous PEEK were heated rapidly to the crystallization temperature and held there one hour. When the cooled samples were subsequently heated in the d.s.c., a small endotherm was reported at a temperature just above the isothermal crystallization temperature (see Figure 3 of ref. 4). Blundell and Osborn attribute this small endotherm to the melting of all of the crystals formed at the isothermal crystallization temperature. The large endotherm at 335°C was then attributed to melting and recrystallization of crystals not present at room temperature. Our results do not support the assignment of the high temperature endotherm to crystals formed solely during the d.s.c. scan. The volume fraction of crystals formed during isothermal crystallization was determined using density and WAXS. In the range of temperatures used by Blundell and Osborn[4], the volume fraction of crystals was about 25–30%. The area under the small endotherm above the crystallization temperature was too small to account for melting of this crystal fraction, whereas very good agreement was obtained with the crystal fraction determined from the high temperature endotherm. An alternative explanation may be provided for the low melting endotherm[9]. Crystallization is very rapid in the temperature range investigated by Blundell and Osborn, hence additional crystallization may occur in their samples through formation of small, imperfect crystals between existing lamellae. These crystals would be very unstable and would melt just above their formation temperature giving rise to a small endothermic response at low temperature.

Rate-dependent crystallization

The importance of high temperature melting for studying the rate dependent crystallization process from the melt was illustrated in *Figure 7*. The thermodynamic melting point of PEEK crystaks is reported at 395°C[4], hence it is necessary to heat the sample above this temperature briefly to remove small nuclei that might act as seed crystals. Both position and height of the crystallization endotherm were affected by the melt temperature.

Rate dependent crystallization has several of the same features as isothermal crystallization. Exothermic response is shown in *Figures 8a,b* for heating and cooling at different rates. In these studies, heat flow was similar to that shown in *Figure 1* for an isothermal crystallization. At constant heating or cooling rate, relative crystallinity develops with temperature as shown in *Figures 9a,b*, giving an S-shaped curve characterized by a fast 'primary' process during the initial stages, and slower 'secondary' processes during the later stages. Because of the strong temperature dependence of the nucleation and growth parameters, crystallization is enhanced as temperature increases or decreases during the non-isothermal scans. Thus, a large fraction of crystallinity develops by the slower, secondary kinetic processes after the maximum in the heat flow curve has been passed, as shown in *Table 3*.

Non-isothermal crystallization during cooling can be analysed using the Ozawa analysis[22]. This is a modification of the Avrami equation that accounts for the effect of heating rate, ϕ, on crystallization from the melt by replacing t (in equation (2)) with T/ϕ. Data are compared at selected temperatures for the various heating rates. The Ozawa equation is:

$$\ln(1-a)=K(T)/\phi^m \qquad (6)$$

where a is the relative crystallinity $[a=X_c(t)/X_c(\infty)]$ and $K(T)$ is the heating function. Results of the Ozawa analysis are shown in *Figure 10*, plotted as $\log(-\ln(1-a))$ vs. $\log\phi$, for temperatures in the range from 275°C to 302.5°C. If the Ozawa treatment correctly models the crystallization process, the plot of $\log(-\ln(1-a))$ vs. $\log\phi$ would result in a series of parallel lines of slope m and intercept $K(T)$. The lines show a distinct curvature, similar to that observed in polyethylene[23], which may be attributed to the effect of secondary crystallization. The changing slopes indicate that m is not constant with temperature during the primary crystallization process. The general curvature seen in *Figure 10* makes it impossible to determine the heating function $K(T)$.

Curvature in the Ozawa plot of $\log[-\ln(1-a)]$ vs. $\log\phi$ sets in when the a values at the chosen temperature include values selected from the primary crystallization process at one rate and the secondary process at another rate. For example, at a temperature of 290°C, the initial portion of the 20°C/min curve overlaps the primary portion of the 10°C/min curve as well as the secondary portion of the 5 and 2°C/min curves. The reason for the curvature in the Ozawa plots has been attributed to secondary kinetic processes[23], but may in fact be also due to the inaccurate assumption of a constant heating function over the entire crystallization process.

It is apparent that the Ozawa analysis does not adequately describe the non-isothermal crystallization kinetics of polymers, like PEEK, in which a large part of the crystallization is attributed to secondary processes[23]. We have adopted a different approach in applying the

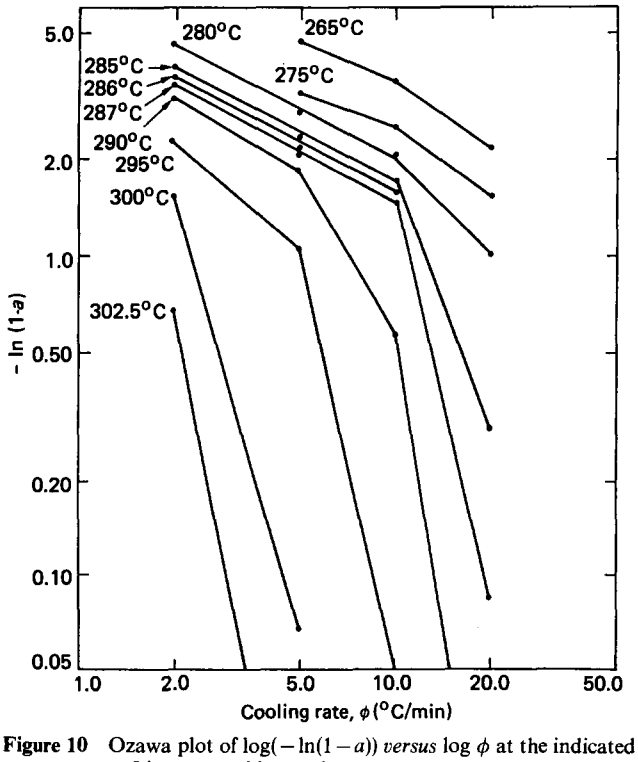

Figure 10 Ozawa plot of $\log(-\ln(1-a))$ *versus* $\log\phi$ at the indicated temperatures. Lines are guides to the eye

Avrami analysis to non-isothermal data. The data shown in *Figure 9*, when plotted as a function of time rather than of temperature, have the same general time dependence at early times as the isothermal data (*Figure 2*). Thus, the initial stages of non-isothermal crystallization can be fit to the Avrami equation, which in its general form (equation (2b)) represents a sigmoidal time dependence. We apply the Avrami analysis to the initial stages of crystallization, at low degree of conversion, where the free spherulitic growth approximation is valid. This is in contrast to the Ozawa analysis which considers constant temperature slices of the crystallinity versus temperature curves, without apparent regard to the mechanism of crystallization.

From *Table 3*, we see that the change from primary to secondary kinetics occurs for degrees of conversion in the range 0.24–0.35 at the faster rates used in this study. We have therefore considered only the smaller degrees of conversion, from $a=0.03$ to $a=0.20$, in applying the Avrami equation to the non-isothermal kinetics. Values of n and k were determined for the non-isothermal kinetics data from the Avrami equation (equation (2b)):

$$\ln(1-a)=-kt^n$$

and are listed in *Table 4* for the heating/cooling rates used here. The non-isothermal crystallization data, when plotted according to equation (2b), yielded a linear relationship for a in the range indicated. From *Table 4* we see that as the magnitude of the heating or cooling rate decreases, the value of k decreases. Values of n are greater than those determined from the isothermal crystallizations, due to changes in the linear growth rate during non-isothermal crystallization, and are more scattered.

The rate constants in *Table 4* can be used to determine an activation energy for crystallization during non-isothermal conditions, at low degree of conversion. We assume that the Avrami parameter k (from equation (2b)) is thermally activated and can be approximately written as:

$$k^{1/n}=k_0\exp(-\Delta E/RT) \qquad (7)$$

where k_0 is a temperature independent preexponential, ΔE is an activation energy, and R and T have their usual meanings. The expression above was evaluated at a very low degree of conversion, $a=0.05$, for all heating/cooling rates. Graphs of $\ln k^{1/n}$ vs. $1/T$ are shown in *Figure 11*. The slope of the curve determines $\Delta E/R$. Activation energy magnitude was found to be 68 kcal mol^{-1} for crystallization from the melt, and 52 kcal mol^{-1} for crystallization from the rubbery amorphous state. (Data for 10°C/min were not used in this calculation.) These activation energies are considerably smaller than the 322 kcal mol^{-1} energy calculated by Kemmish and Hay[11] for isothermal cold crystallization.

Table 4 Parameters k and n for non-isothermal crystallization of PEEK, at degree of conversion $0.03<a<0.20$

Rate, ϕ (°C/min)	k^a	n	$k^{1/n}$ (s^{-1})
−20	2.5×10^{-9}	5.4	0.026
−10	7.2×10^{-10}	5.1	0.016
−5	3.5×10^{-10}	4.6	0.0088
−2	1.2×10^{-13}	5.4	0.0040
−1	6.1×10^{-12}	4.4	0.0028
+50	1.8×10^{-7}	5.1	0.047
+20	4.7×10^{-10}	5.7	0.023
+10	1.6×10^{-8}	4.7	0.022
+5	6.6×10^{-16}	6.9	0.0063
+2	7.7×10^{-19}	7.5	0.0038
+1	2.9×10^{-21}	7.8	0.0023

[a] Determined from equation (2b)

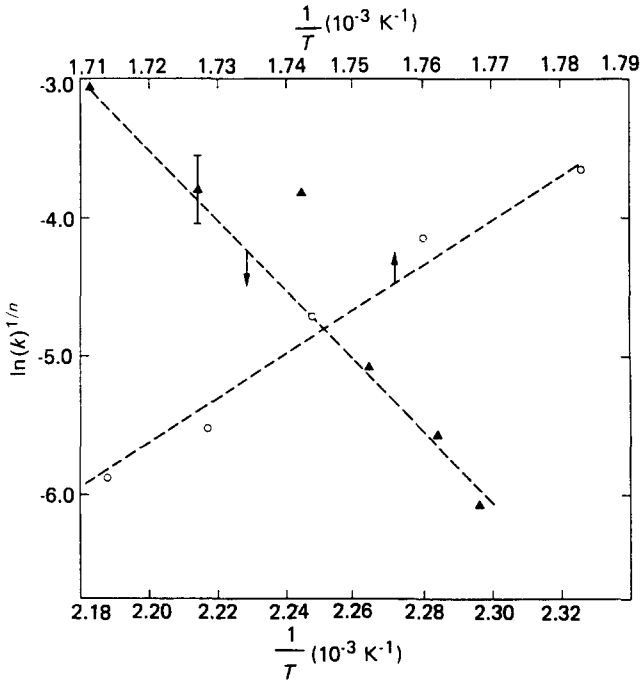

Figure 11 $\ln(k)^{1/n}$ vs. $1/T$ for Avrami parameter k deduced from non-isothermal crystallization data: (○), cooling from the melt; (▲), heating the rubbery amorphous state. Lines are guides to the eye

It is useful to compare our results of PEEK activation energy to those of PET[15–17,20,24]. Several groups have derived activation energies for isothermal crystallization of PET by a variety of methods. In early work Cobbs and Burton[24] crystallized PET from the rubbery amorphous state. From 120°C to 240°C, they determined an activation energy of 20 kcal mol^{-1}. Mayhan *et al.*[17] studied crystallization from the rubbery amorphous state in the temperature range 25°C–240°C. Activation energy derived using first order kinetics and crystallization half-life was 37 kcal mol^{-1}. Miller crystallized the rubbery state from 100°C to 115°C, and obtained activation energy of 44 kcal mol^{-1} by the same approach. Villanova *et al.*[17], used low molecular weight PET fractions and crystallized from the melt. They obtained crystallization rates from the slope of a vs. t curves for a in the range 0.1 to 0.7. These rates were used to calculate activation energies ranging from 44 to 72 kcal mol^{-1}.

Porter's group has determined activation energy for non-isothermal crystallization from the rubbery amorphous state[20]. Undrawn PET samples had activation energies ranging from 38–59 kcal mol^{-1}. Our activation energies for PEEK are comparable to those of PET, whether determined using isothermal or non-isothermal crystallization. Energies for melt crystallization were smaller in magnitude than for crystallization from the rubbery state.

CONCLUSIONS

PEEK has been shown to follow an Avrami behaviour during isothermal crystallization from the melt and from the rubbery amorphous state. The Avrami exponent n was about three, which is consistent with heterogeneous nucleation and three dimensional spherulitic growth. Growth rate parameters derived from exothermic heat flow during melt crystallization are in good agreement with the results of Blundell and Osborn[4] which were obtained using a different method.

Cold crystallization from the rubbery amorphous state occurs at low temperatures during d.s.c. scans, depending upon the previous thermal history of the sample. Melt crystallization at high temperatures followed by fast quenching results in material that may still undergo further crystallization at low temperature. Samples cooled from the melt very slowly show no tendency to crystallize at low temperature. Successive thermal cycling of originally quenched amorphous material is followed by cold crystallization at temperatures up to 250°C.

Non-isothermal crystallizations from the melt and from the rubbery amorphous state showed that a very large fraction of relative crystallinity develops after the maximum in the heat flow curve, where the kinetics are changing to a slower process. The Ozawa analysis[22], when applied to this system, failed to describe the primary crystallization process. This was a result of inaccurate assumption of constant heating function, $K(T)$, and constant exponent, m. We have presented a different analysis based on the observation that, at a given heating/cooling rate, crystallinity develops with a time dependence that is sigmoidal at low degree of conversion. The parameters n and k associated with a particular rate were indeed constant for degrees of conversion from 0.03 to 0.20 where the primary process alone governs crystallization. The upper limit on the degree of conversion was determined approximately as the relative crystallinity that had developed by the maximum in the exothermic heat flow curve. This approach should be generally applicable to the study of non-isothermal crystallization kinetics in polymers having a large fraction of secondary crystallization. The rate constant k can then be used to determine activation energies during non-isothermal crystallization.

ACKNOWLEDGEMENTS

Discussions with Drs Robert Fedors and Amitava Gupta are greatly appreciated. The research described in this paper was performed at the Jet Propulsion Laboratory, California Institute of Technology, while the principal author held a NASA-NRC Resident Research Associateship Award. Research was sponsored by National Aeronautics and Space Administration through Langley Research Center.

REFERENCES

1 ICI Fourth Edition, Provisional Data Sheet PK PDI 'Victrex PEEK' Aromatic Polymer Grades, Properties and Processing Characteristics, Imperial Chemical Industries PLC, March 1982
2 Attwood, T. E., Dawson, P. C., Freeman, J. L., Hay, L. R. J., Rose, J. B. and Staniland, P. A. *Polymer* 1981, **22**, 1096
3 Bishop, M. T., Karasz, F. E., Russo, P. S. and Langley, K. H. *Macromolecules* 1985, **18**, 86
4 Blundell, D. J. and Osborn, B. N. *Polymer* 1983, **24**, 953
5 Hay, J. N., Kemmish, D. J., Langford, J. I. and Rae, A. I. M. *Polymer* 1984, **29** (*Commun.*), 175
6 Dawson, P. C. and Blundell, D. J. *Polymer* 1980, **21**, 577
7 Lovinger, A. J. and Davis, D. D. *J. Appl. Phys.* 1985, **58**, 2843
8 Avrami, M. *J. Chem. Phys.* 1934, **7**, 1103; Avrami, M. *J. Chem. Phys.* 1940, **8**, 212
9 Morgan, L. B. *J. Appl. Chem.* 1954, **4**, 160
10 Cebe, P., Gupta, A. and Yavrouian, A. (to be published)
11 Kemmish, D. J. and Hay, J. N. *Polymer* 1985, **26**, 905
12 Hoffman, J. D. and Lauritzen, J. I. *J. Res. Nat. Bur. Stand.* 1961, **65A**, 297; Hoffman, J. D., Davis, G. T. and Lauritzen, J. I. 'Treatise on Solid State Chemistry', (Ed. N. B. Hanney), Plenum Press, New York, 1976, Vol. 3
13 Suzuki, T. and Kovacs, A. J. *Polym. J.* 1970, **1**, 82
14 Palys, L. H. and Phillips, P. J. *J. Polym. Sci., Polym. Phys. Edn.* 1980, **18**, 829
15 Villanova, P., Ribas, S. and Guzman, G. *Polymer* 1985, **26**, 423
16 Miller, B. *J. Appl. Polym. Sci.* 1967, **11**, 2343
17 Mayhan, K. G., James, W. J. and Bosch, W. J. *Appl. Polym. Sci.* 1965, **9**, 3605
18 Holdsworth, P. J. and Turner-Jones, A. *Polymer* 1971, **12**, 195
19 Wunderlich, B. 'Macromolecular Physics', Academic Press, New York, 1980, Vol. 3, p. 191
20 Sun, T., Periera, J. and Porter, R. S. *J. Polym. Sci., Polym. Phys. Edn.* 1984, **22**, 1163
21 Lin, C. C. *Polym. Eng. Sci.* 1983, **23**, 113
22 Ozawa, T. *Polymer* 1971, **12**, 150
23 Eder, M. and Wlochowicz, A. *Polymer* 1983, **24**, 1593
24 Cobbs, W. H. and Burton, R. L. *J. Polym. Sci.* 1953, **10**, 275